

# Identification of Strongly Correlated Spin Liquid in Herbertsmithite

V. R. SHAGINYAN<sup>1,2 (a)</sup>, A. Z. MSEZANE<sup>2</sup>, K. G. POPOV<sup>3</sup>, G. S. JAPARIDZE<sup>2</sup> and V. A. STEPHANOVICH<sup>4</sup>

<sup>1</sup> Petersburg Nuclear Physics Institute, Gatchina, 188300, Russia

<sup>2</sup> Clark Atlanta University, Atlanta, GA 30314, USA

<sup>3</sup> Komi Science Center, Ural Division, RAS, Syktyukar, 167982, Russia

<sup>4</sup> Opole University, Institute of Physics, Opole, 45-052, Poland

PACS 75.40.Gb – Spin dynamics  
 PACS 64.70.Tg – Quantum phase transitions  
 PACS 71.10.Hf – Non-Fermi-liquid ground states  
 PACS 76.60.Es – Spin-lattice relaxation

**Abstract.** - Exotic quantum spin liquid (QSL) is formed with such hypothetical particles as fermionic spinons carrying spin  $1/2$  and no charge. Here we calculate its thermodynamic and relaxation properties. Our calculations unveil the fundamental properties of QSL, forming strongly correlated Fermi system located at a fermion condensation quantum phase transition. These are in a good agreement with experimental data and allow us to detect the behavior of QSL as that observed in heavy fermion metals. We predict that the thermal resistivity of QSL under the application of magnetic fields at fixed temperature demonstrates a very specific behavior. The key features of our findings are the presence of spin-charge separation and QSL formed with itinerant heavy spinons in herbertsmithite.

A search for the materials formed with fermionic spinons carrying spin  $1/2$  and no charge is a challenge for a condensed matter physics [1]. A quantum spin liquid (QSL) can be viewed as an exotic quantum state of matter composed of hypothetical particles like chargeless fermionic spinons with spin  $1/2$  and having a possibility to fluctuate as in ordinary fluid. The advances in theoretical studies of QSLs date back to Anderson's seminal paper [2] which ignited hot discussions in the scientific community. Theoretical consensus is that the ground state of QSLs is not magnetically ordered, including both gapped and gapless spin liquids [1]. However, the experimental investigation of QSLs is hindered by a lack of real solids where it can occur. In other words, no specific model substances with QSL has been found yet, although there are few possible candidates. This means that the recognition of a perfect material with clear QSL realization makes a major challenge in modern condensed matter physics.

The experimental studies of herbertsmithite  $\text{ZnCu}_3(\text{OH})_6\text{Cl}_2$  single crystal have found no evidences of long range magnetic order or spin freezing indicating that

$\text{ZnCu}_3(\text{OH})_6\text{Cl}_2$  is the promising system to investigate QSL [3–12]. Presently herbertsmithite  $\text{ZnCu}_3(\text{OH})_6\text{Cl}_2$  has been exposed as a  $S = 1/2$  Heisenberg antiferromagnet [3] on a perfect kagome lattice and new experimental investigations have revealed its unusual behavior [4–7], see Ref. [8] for a recent review. In  $\text{ZnCu}_3(\text{OH})_6\text{Cl}_2$ , the  $\text{Cu}^{2+}$  ions with  $S = 1/2$  form the triangular kagome lattice, and are separated by nonmagnetic intermediate layers of Zn and Cl atoms. The planes of the  $\text{Cu}^{2+}$  ions can be considered as two-dimensional (2D) layers with negligible magnetic interactions along the third dimension.

A frustration of simple kagome lattice leads to a dispersionless topologically protected branch of the spectrum with zero excitation energy known as the flat band [13,14]. In this case the fermion condensation quantum phase transition (FCQPT) [15,16] can be considered as quantum critical point (QCP) of the  $\text{ZnCu}_3(\text{OH})_6\text{Cl}_2$  QSL composed of chargeless fermions with  $S = 1/2$  occupying the corresponding Fermi sphere with the Fermi momentum  $p_F$ . As we are dealing with the 3D compound  $\text{ZnCu}_3(\text{OH})_6\text{Cl}_2$  rather than with an ideal 2D kagome lattice, we have to bear in mind that the real magnetic interactions in the substance can shift the QSL from the exact FCQPT point,

<sup>(a)</sup>Email: vrshag@thd.pnpi.spb.ru

positioning it in front of or behind the QCP. Therefore, the actual location has to be established by analyzing the experimental data only. It is believed that the  $S = 1/2$  model on the kagome lattice can be viewed as a gapless spin liquid [4–12], while recent accurate calculations point to a fully gapped one, see [17] and Refs. therein. Thus, it is of crucial importance to test what kind of QSL is formed in herbertsmithite and determines its low temperature thermodynamic and relaxation properties.

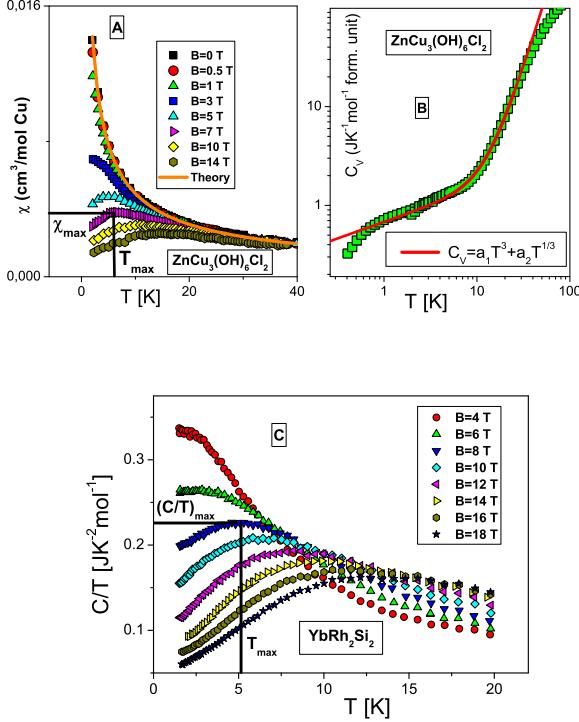


Fig. 1: Panel A:  $T$ -dependence of the magnetic susceptibility  $\chi$  at different magnetic fields  $B$  [6] shown in the legend. The values of  $\chi_{\max}$  and  $T_{\max}$  at  $B = 7$  T are also shown. Our calculations at  $B = 0$  are depicted by the solid curve  $\chi(T) \propto T^{-\alpha}$  with  $\alpha = 2/3$ . Panel B: The heat capacity measured on  $\text{ZnCu}_3(\text{OH})_6\text{Cl}_2$  at zero magnetic field [5] is shown by squares. Solid curve corresponds to our theoretical approximation based on the function  $C = a_1T^3 + a_2T^{1/3}$  with fitting parameters  $a_1$  and  $a_2$ , see eq. (9). Panel C reports the  $T$ -dependence of the electronic specific heat  $C/T$  of  $\text{YbRh}_2\text{Si}_2$  at different magnetic fields [21] as shown in the legend. The values of  $(C/T)_{\max}$  and  $T_{\max}$  at  $B = 8$  T are also shown.

To identify unambiguously the compound having an exotic QSL located at FCQPT, we must analyze a multitude of experimental features rather than a single one. At very low temperatures and with magnetic field  $B$  applied, we expect that the possible QSL substances reveal a Landau Fermi-liquid (LFL) behavior of their physical characteristics, like the magnetic specific heat and susceptibility, spin-lattice relaxation rate and the heat transport coef-

ficients. At the same time, at elevated temperatures a non-Fermi liquid (NFL) regime emerges separated by a transition (or crossover) region. In other words, the candidate substance should exhibit the LFL, NFL and the transition regimes similar to the case of heavy fermion (HF) metals and 2D  $^3\text{He}$  [15, 16, 18, 19]. This means that QSL plays the role of HF liquid placed into the insulating compound. Spin is carried by an electron which becomes localized, while the spin is itinerant. Such a behavior resembles the spin-charge separation observed recently in 1D system of interacting non-localized electrons [20]. In our case the charges is completely localized while the spins are itinerant dwelling on the topologically protected branch. As a result, we face a breathtaking picture: New particles govern the systems properties at low temperatures and these are different from the particles presented in the Hamiltonian describing the system.

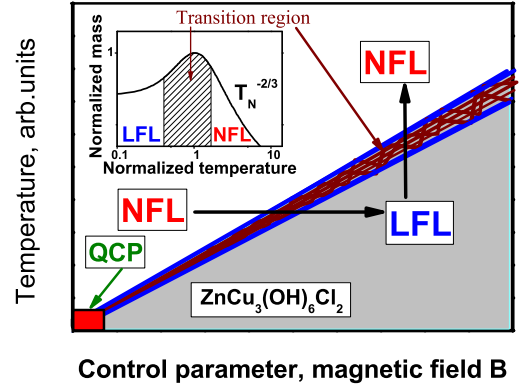


Fig. 2: Schematic phase diagram of  $\text{ZnCu}_3(\text{OH})_6\text{Cl}_2$ . The square at the origin shown by the arrow represents QCP near which QSP is located. Vertical and horizontal arrows show LFL-NFL and NFL-LFL transitions at fixed  $B$  and  $T$  respectively. At fixed  $T$  the increase of  $B$  drives the system along the horizontal arrow from NFL regime to LFL one. On the contrary, at fixed  $B$  and raising temperatures the system transits along the vertical arrow from LFL regime to NFL one. The inset demonstrates the behavior of the normalized effective mass  $M_N^*$  versus normalized temperature  $T_N$  as given by eq. (5). It is seen that temperatures  $T_N \sim 1$  signify a transition region between the LFL regime with almost constant effective mass and NFL one, given by  $T^{-2/3}$  dependence. It is seen from eq. (5) that the width of the transition region  $T_w \propto T \propto B$ . The transition region, where  $M_N^*$  reaches its maximum at  $T/T_{\max} = 1$ , is shown by the arrows and hatched area both in the main panel and in the inset.

We begin with the analysis of the magnetic susceptibility  $\chi(T)$  of  $\text{ZnCu}_3(\text{OH})_6\text{Cl}_2$  shown in the panel A of fig. 1. It displays an unusual behavior [6]: at  $B \geq 3$  T,  $\chi(T)$  has a maximum  $\chi_{\max}(T)$  at some temperature  $T_{\max}(B)$ . The maximum  $\chi_{\max}(T)$  decreases as magnetic field  $B$  grows,

while  $T_{\max}(B)$  shifts to higher  $T$  reaching 15 K at  $B = 14$  T. It is seen from the panel A of fig. 1 that  $\chi(T) \propto T^{-\alpha}$  with  $\alpha = 2/3$ . The calculated exponent is in good agreement with the experimental value  $\alpha = 2/3 \simeq 0.66$  [6]. The observed behavior of  $\chi$  strongly resembles that in HF metals and associated with their proximity to FCQPT [15,16]. The specific heat  $C$ , arising from the Cu spin system, at the lowest explored temperatures,  $106 < T < 400$  mK, follows a linear temperature dependence,  $C \propto T$ . As it is seen from fig. 1, panel B, for temperatures of a few Kelvin and higher, the specific heat becomes  $C(T) \propto T^3$  and is dominated by the lattice contribution. At low temperatures  $T \leq 1$  K, the strong magnetic field dependence of the specific heat  $C$  suggests that it is predominately formed by the specific heat  $C_{mag}$  of QSL,  $C_{mag} = C - a_1 T^3$ , since the lattice contribution is independent of  $B$  [4–6]. The above behavior of  $\chi$  (fig. 1, panel A) is a visible parallel to that of the HF metal  $\text{YbRh}_2\text{Si}_2$  observed in measurements of  $C/T$  and displayed in the panel C. This coincidence becomes evident if we recollect that for HF liquid  $\chi \propto C/T$  [15]. It is seen from the panel C that the electronic specific heat of  $\text{YbRh}_2\text{Si}_2$  [21] is also strongly dependent on the applied magnetic field and we will see below that both the specific heat  $C_{mag}$  and that of  $\text{YbRh}_2\text{Si}_2$  exhibit the same behavior.

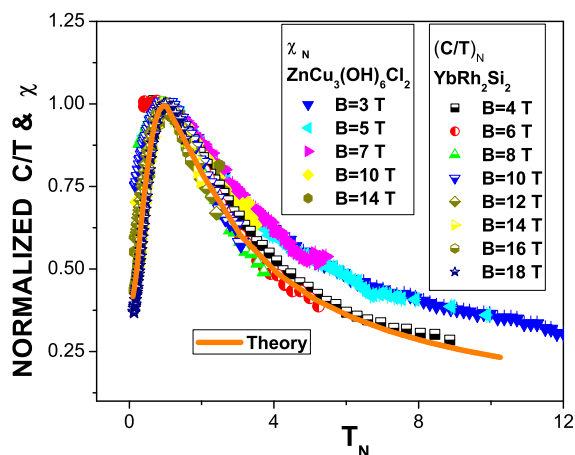


Fig. 3: The experimental data on measurements of  $\chi_N$  [6],  $(C/T)_N = M_N^*$  [21] and our calculations of  $M_N^*$  at fixed high magnetic field (high means that it polarizes completely the quasiparticles spins) are shown by points of different shape and solid curve respectively. It is clearly seen that the data collected on both  $\text{ZnCu}_3(\text{OH})_6\text{Cl}_2$  and  $\text{YbRh}_2\text{Si}_2$  merge into the same curve, obeying the scaling behavior. In accordance with the phase diagram displayed in the panel A, at growing temperatures ( $y \simeq 1$ ) the LFL regime first converts into the transition one and then disrupts into the NFL regime. This demonstrates that the spin liquid of herbertsmithite is close to QCP and behaves like HF liquid of  $\text{YbRh}_2\text{Si}_2$  in strong magnetic fields [25].

To study theoretically the low temperature thermodynamic, relaxation and scaling properties of herbertsmithite, we use the model of homogeneous HF liquid [15]. This model permits to avoid complications associated with the crystalline anisotropy of solids. In our case, similar to the above HF liquid, QSL is composed of chargeless fermions (spinons) with  $S = 1/2$  occupying the corresponding two Fermi spheres with the Fermi momentum  $p_F$ . The ground state energy  $E(n)$  is given by the Landau functional depending on the quasiparticle distribution function  $n_\sigma(\mathbf{p})$ , where  $p$  is the momentum and  $\sigma$  is the spin index. The effective mass  $M^*$  is governed by the Landau equation [15, 22]

$$\frac{1}{M^*(T, B)} = \frac{1}{M^*} + \frac{1}{p_F^2} \sum_{\sigma_1} \int \frac{\mathbf{p}_F \mathbf{p}_1}{p_F} \times F_{\sigma, \sigma_1}(\mathbf{p}_F, \mathbf{p}_1) \frac{\partial \delta n_{\sigma_1}(\mathbf{p}_1, T, B)}{\partial p_1} \frac{dp_1}{(2\pi)^3}. \quad (1)$$

Here we rewrite the quasiparticle distribution function as  $n_\sigma(\mathbf{p}, T, B) \equiv n_\sigma(\mathbf{p}, T = 0, B = 0) + \delta n_\sigma(\mathbf{p}, T, B)$ . The Landau amplitude  $F$  is completely defined by the fact that the system has to be at QCP of FCQPT [15, 23–25], see [25] for details of solving eq. (1). The sole role of Landau amplitude is to bring the system to FCQPT point, where Fermi surface alters its topology so that the effective mass acquires temperature and field dependencies. At this point, the term  $1/M^*$  vanishes, eq. (1) becomes homogeneous and can be solved analytically [15, 23]. At  $B = 0$ , the effective mass, being strongly  $T$ -dependent, demonstrates the NFL behavior given by eq. (1)

$$M^*(T) \simeq a_T T^{-2/3}. \quad (2)$$

At finite  $T$ , under the application of magnetic field  $B$  the two Fermi spheres due to the Zeeman splitting are displaced by opposite amounts, the final chemical potential  $\mu$  remaining the same within corrections of order  $B^2$ . As a result, field  $B$  drives the system to LFL region, and again it follows from eq. (1) that

$$M^*(B) \simeq a_B B^{-2/3}. \quad (3)$$

It is seen from eqs. (2) and (3) that effective mass diverges at FCQPT. At finite  $B$  and  $T$  near FCQPT, the solutions of eq. (1)  $M^*(B, T)$  can be well approximated by a simple universal interpolating function. This interpolation occurs between the LFL regime, given by eq. (3) and NFL regime given by eq. (2) [15, 23]. In the case of strongly correlated Fermi systems like HF metals and 2D  $^3\text{He}$  the thermodynamic and relaxation properties are defined by the effective mass  $M^*$ , namely  $\chi \propto (C/T) \propto \sqrt{1/T_1 T} \propto M^*$ , where  $1/T_1 T \propto \chi^2$  is the spin-lattice relaxation rate [15]. To study the universal scaling behavior of strongly correlated Fermi system, it is convenient to introduce the normalized effective mass  $M_N^*$  and the normalized temperature  $T_N$  dividing the effective mass  $M^*$  and temperature  $T$  by their maximal values,  $M_M^*$  and  $T_M$  respectively. The

behavior of  $M_N^* = M^*/M_M^*$  as a function of  $y = T/T_M$  shown in the inset to fig. 2 is independent of the specific features of corresponding strongly correlated Fermi system, while both  $M_M^*$  and  $T_M$  are determined by these features [15]. As a result, we obtain [15]

$$\chi_N = (C_{mag}/T)_N = \left(\sqrt{1/T_1 T}\right)_N = M_N^*, \quad (4)$$

where  $\chi_N$ ,  $(C/T)_N$  and  $(\sqrt{1/T_1 T})_N$  are the normalized values of  $\chi$ ,  $C/T$  and  $\sqrt{1/T_1 T}$ , respectively. As a typical example, the corresponding maximum values  $\chi_{max}$ ,  $(C/T)_{max}$  and  $T_{max}$  used to normalize the susceptibility  $\chi$  and  $C/T$  are shown in fig. 1, the panels A and C. We note that our calculations of  $M_N^*$  based on eq. (1) do not contain any fitting parameters. The normalized effective mass  $M_N^* = M^*/M_M^*$  as a function of the normalized temperature  $y = T_N = T/T_M$  reads

$$M_N^*(y) \approx c_0 \frac{1 + c_1 y^2}{1 + c_2 y^{8/3}}. \quad (5)$$

Here  $c_0 = (1 + c_2)/(1 + c_1)$ ,  $c_1$  and  $c_2$  are fitting parameters, approximating the Landau amplitude. Since magnetic field  $B$  enters eq. (1) only in combination  $B\mu_B/T$ , we have  $T_{max} \propto B\mu_B$  [15, 23], where  $\mu_B$  is the Bohr magneton. Thus, for finite magnetic fields variable  $y$  becomes

$$y = T/T_N \propto T/\mu_B B. \quad (6)$$

Subsequently we use eq. (5) to clarify our calculations based on eq. (1). The variables  $B$  and  $T$  enter eq. (1) symmetrically, therefore eq. (5) determines  $M^*$  as a function of  $B$  at fixed  $T$  [15]. It follows directly from eqs. (3), (5) and (1) that

$$\chi(T/\mu_B B) T^{2/3} \simeq \chi(T, B) T^{0.66} \propto y^{2/3} M_N^*(y). \quad (7)$$

Since the magnetization  $M(T, B) = \int \chi(T, b) db$ , we obtain that

$$M(T, B) T^{-1/3} \simeq M(T, B) T^{-0.34} \quad (8)$$

depends on the only variable  $y$ . Equations (7) and (8) confirm the scaling behavior of both  $\chi T^{0.66}$  and  $MT^{-0.34}$  experimentally established in Ref. [6]

Now we construct the schematic phase diagram of  $\text{ZnCu}_3(\text{OH})_6\text{Cl}_2$ . This is reported in fig. 2. At  $T = 0$  and  $B = 0$  the system is located near FCQPT without tuning. In fact, it is located in front of FCQPT since  $C(T)$  demonstrates the LFL behavior characterized by the linear  $T$ -dependence at low temperatures [4]. Both magnetic field  $B$  and temperature  $T$  play role of the control parameters, driving the system from NFL to LFL regions as shown by the vertical and horizontal arrows. It follows from fig. 3 that in accordance with eq. (4) the behavior of  $\chi_N$  coincides with that of  $(C/T)_N$  in  $\text{YbRh}_2\text{Si}_2$ . Figure 4, the right and left panels correspondingly, demonstrates that eqs. (6) and (3) are in a good agreement with the experimental facts.

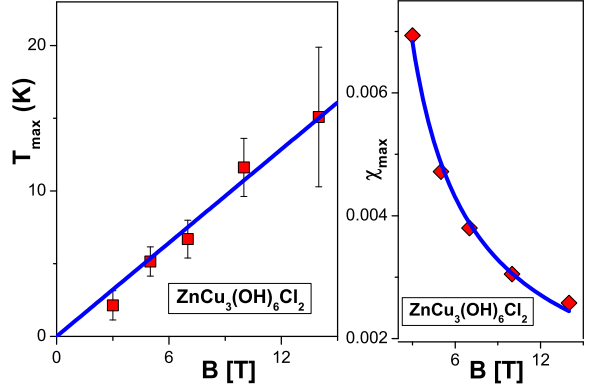


Fig. 4: Left panel: The temperatures  $T_{max}(B)$  at which the maxima of  $\chi$  (see fig. 1, the panel A) are located. The solid line represents the function  $T_{max} \propto aB$ ,  $a$  is a fitting parameter, see eq. (6). Right panel: the maxima  $\chi_{max}$  of the functions  $\chi(T)$  versus magnetic field  $B$  (see fig. 1, the panel A). The solid curve is approximated by  $\chi_{max}(B) = dB^{-2/3}$ , see eq. (3),  $d$  is a fitting parameter.

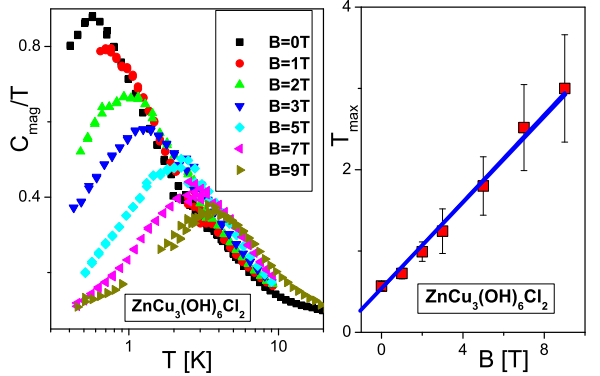


Fig. 5: Left panel: The specific heat  $C_{mag}/T$  of QSL given by eq. (9) is extracted from measurements of  $C(B)$  on  $\text{ZnCu}_3(\text{OH})_6\text{Cl}_2$  at different magnetic fields shown in the legend [5]. Right panel: The temperatures  $T_{max}(B)$  at which the maxima of  $C_{mag}/T$  (see the left panel) are located. The solid line represents the function  $T_{max} \propto B$ , see eq. (6).

According to eq. (4), in the case of QSL the behavior of the specific heat  $(C_{mag}/T)_N$  must coincide with that of  $\chi_N$ . To separate  $C_{mag}$  contribution, we approximate the general specific heat  $C(T)$  at  $T > 2$  K by the function

$$C(T) = a_1 T^3 + a_2 T^{1/3}, \quad (9)$$

where the first term proportional to  $a_1$  is due to the lattice (phonon) contribution and the second one is determined by the QSL when QSL exhibits the NFL behavior as it follows from eq. (2). It is seen from fig. 1, the panel B, that the approximation is valid in the wide temperature

range. We note that the value of  $a_1$  is almost independent of  $a_2$ , the presence of which allows us to achieve a better approximation for  $C$ . The obtained heat capacity  $C_{mag}/T = (C - a_1 T^3)/T$  is displayed in the left panel of fig. 5, while the right panel B demonstrates the maximum temperature as a function of the magnetic field  $B$ . It is seen that  $C_{mag}/T \propto M^*$  behaves like  $\chi \propto M^*$  shown in fig. 1, the panel A. In figs. 6 and 7, the normalized  $(C_{mag}/T)_N$  and  $\chi_N$  are depicted. It is seen from both these figures that the results obtained on different samples and measurements [4, 5] exhibit similar properties. As it is seen from figs. 3, 6 and 7 that in accordance with eq. (4),  $(C_{mag}/T)_N \simeq \chi_N$  displays the same scaling behavior as  $(C/T)_N$  measured on the HF metal YbRh<sub>2</sub>Si<sub>2</sub>. Therefore, the scaling behavior of the thermodynamic functions of herbertsmithite is the intrinsic feature of the compound and has nothing to do with magnetic impurities. This observation rules out a possible supposition that extra Cu spins outside the kagome planes considered as paramagnetic weakly interacting impurities could be responsible for the divergent behavior of the susceptibility at low temperatures seen from fig. 1, the panel A. In that case the supposition is to lead to explanations of the observed scaling behavior of  $\chi$  and  $C/T$  in magnetic fields shown in figs. 3, 6 and 7. Obviously, it is impossible.

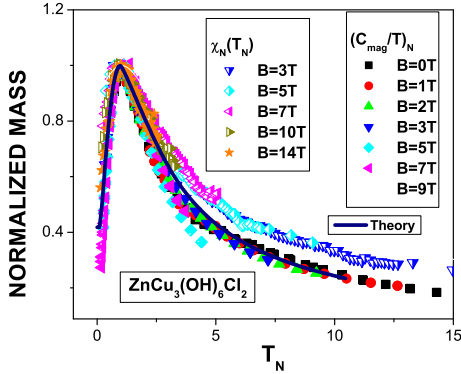


Fig. 6: The normalized susceptibility  $\chi_N = \chi/\chi_{\max} = M_N^*$  and the normalized specific heat  $(C_{mag}/T)_N = M_N^*$  of QSL effective mass versus normalized temperature  $T_N$  as a function of the magnetic fields shown in the legends.  $\chi_N$  is extracted from the measurements of the magnetic susceptibility  $\chi$  in magnetic fields  $B$  [6] shown in the panel A of fig. 1. The normalized specific heat is extracted from the data displayed in fig. 5, the left panel. Our calculations are depicted by the solid curve tracing the scaling behavior of  $M_N^*$ .

Figure 8 displays the normalized spin-lattice relaxation rates  $(1/T_1 T)_N$  at fixed temperature versus normalized magnetic field  $B_N$ . We notice from fig. 8 that the magnetic field  $B$  progressively reduces  $1/T_1 T$ , and the spin-lattice relaxation rate as a function of  $B$  possesses an inflection point at some  $B = B_{inf}$  shown by the arrow.

To clarify the scaling behavior in that case, we normalize both the function  $1/T_1 T$  and the magnetic field. Namely, we normalize  $(1/T_1 T)$  by its value at the inflection point, and magnetic field is normalized by  $B_{inf}$ ,  $B_N = B/B_{inf}$ . It follows from eq. (4) that  $(1/T_1 T)_N = (M_N^*)^2$  and we expect that different strongly correlated Fermi systems located near FCQPT exhibit the same behavior of the normalized spin-lattice relaxation rate [15]. It is seen from fig. 8, that both herbertsmithite ZnCu<sub>3</sub>(OH)<sub>6</sub>Cl<sub>2</sub> [26] and HF metal YbCu<sub>5-x</sub>Au<sub>x</sub> [27] demonstrate similar behavior of the normalized spin-lattice relaxation rate. As seen from fig. 8, at  $B \leq B_{inf}$  (or  $B_N \leq 1$ ) the normalized relaxation rate  $(1/T_1 T)_N$  depends weakly on the magnetic field, while at higher fields  $(1/T_1 T)_N$  diminishes in agreement with eq. (3),  $(1/T_1 T)_N = (M_N^*)^2 \propto B^{-4/3}$ . Thus, in accordance with the phase diagram shown in fig. 2, we conclude that the application of magnetic field  $B$  leads to crossover from the NFL to LFL behavior and to the significant reduction in the relaxation rate.

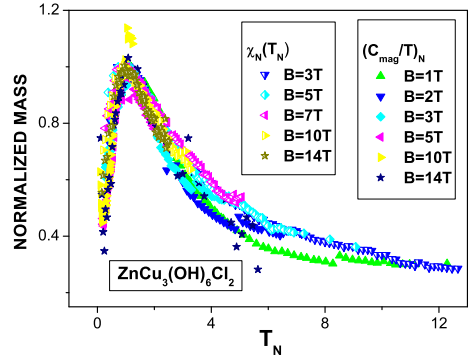


Fig. 7: The normalized susceptibility  $\chi_N$  and the normalized specific heat  $(C_{mag}/T)_N$  of QSL effective mass versus normalized temperature  $T_N$  as a function of the magnetic fields shown in the legends.  $\chi_N$  and  $(C_{mag}/T)_N$  are extracted from the data of [6] and [4], respectively.

As it was mentioned above, QSL plays a role of HF liquid framed into the insulating compound. Thus, we expect that QSL in herbertsmithite behaves like the electronic liquid in HF metals if the charge of an electron were zero. In that case, the thermal resistivity  $w = LT/\kappa$ ,  $w = w_0 + A_w T^2$ , of QSL behaves like the electrical resistivity  $\rho = \rho_0 + A_\rho T^2$  of the electronic liquid, since  $A_w$  represents the contribution of spinon-spinon scattering to thermal transport, being analogous to the contribution  $A_\rho$  to charge transport by electron-electron scattering. Here,  $L$  is the Lorenz number,  $\kappa$  is the thermal conductivity of QSL,  $\rho_0$  and  $w_0$  are residual resistivity of the electronic liquid and QSL, respectively, and coefficient  $A_w \sim A_\rho \propto (M^*)^2$  [15, 28]. Thus, we predict that the coefficient  $A_w$  of the thermal resistivity of QSL under the application of magnetic fields at fixed temperature be-

haves like the spin-lattice relaxation rate shown in fig. 8,  $A_w(B) \propto 1/T_1 T(B) \propto (M^*(B))^2$ , while in the LFL region at fixed magnetic fields the thermal conductivity is a linear function of temperature,  $\kappa \propto T$ .

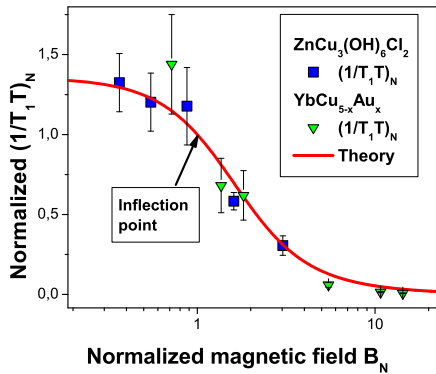


Fig. 8: The relaxation properties of herbertsmithite versus those of HF metals. The normalized spin-lattice relaxation rate  $(1/T_1 T)_N$  at fixed temperature as a function of magnetic field: Solid squares correspond to data on  $(1/T_1 T)_N$  extracted from measurements on  $\text{ZnCu}_3(\text{OH})_6\text{Cl}_2$  [26], while the solid triangles correspond to those extracted from measurements on  $\text{YbCu}_{5-x}\text{Au}_x$  with  $x = 0.4$  [27]. The inflection point where the normalization is taken is shown by the arrow. Our calculations based on eq. (1) are depicted by the solid curve tracing the scaling behavior of  $(M_N^*)^2$ .

To conclude, we have calculated the thermodynamic and relaxation properties of herbertsmithite. Our calculations unveil the fundamental properties of QSL, forming strongly correlated Fermi system located at FCQPT. These are in a good agreement with experimental data and allow us to detect the behavior of QSL as that observed in heavy fermion metals. The key features of our findings are the presence of spin-charge separation and QSL formed with itinerant heavy spinons in herbertsmithite. Herbertsmithite represents a fascinating experimental example when the new particles-spinons, non-existing as free ones, totally replace the initial particles entering the Hamiltonian to dominate the properties at low temperatures. It is highly desirable to perform the detailed experimental studies of the transport properties of herbertsmithite. Also, conditions for spinons to form a superfluid liquid remain to be explored.

We are grateful to V. A. Khodel for valuable discussions and to A. Harrison and M. A. de Vries for their help in dealing with the experimental data [5]. This work was supported by U.S. DOE, Division of Chemical Sciences, Office of Basic Energy Sciences, Office of Energy Research, AFOSR and the RFBR # 12-02-00017.

## REFERENCES

- [1] BALENTS L., *Nature*, **464** (2010) 199.
- [2] ANDERSON P. W., *Mater. Res. Bull.*, **8** (1973) 153.
- [3] SHORES M. P., NYTKO E. A., BARTLETT B. M. and NOCERA D. G., *J. Am. Chem. Soc.*, **127** (2005) 13462.
- [4] HELTON J. S. *et al.*, *Phys. Rev. Lett.*, **98** (2007) 107204.
- [5] DE VRIES M. A., KAMENEV K. V., KOCKELMANN W. A., SANCHEZ-BENITEZ J. and HARRISON A., *Phys. Rev. Lett.*, **100** (2008) 157205.
- [6] HELTON J. S. *et al.*, *Phys. Rev. Lett.*, **104** (2010) 147201.
- [7] HAN T. H. *et al.*, *Phys. Rev. B*, **83** (2011) 100402(R).
- [8] BERT F. and MENDELS P., *J. Phys. Soc. Jpn.*, **79** (2010) 011001.
- [9] LEE S. and LEE P. U., *Phys. Rev. Lett.*, **95** (2005) 036403.
- [10] MOTRUNICH O. I., *Phys. Rev. B*, **72** (2005) 045105.
- [11] RAN Y., HERMELE M., LEE P. A. and WEN X.-G., *Phys. Rev. Lett.*, **98** (2007) 117205.
- [12] RYU S., MOTRUNICH O. I., ALICEA J. and FISHER M. P. A., *Phys. Rev. B*, **75** (2007) 184406.
- [13] GREEN D., SANTOS L. and CHAMON C., *Phys. Rev. B*, **82** (2010) 075104.
- [14] HEIKKILÄ T. T., KOPNIN N. B. and VOLOVIK G. E., *JETP Lett.*, **94** (2011) 233.
- [15] SHAGINYAN V. R., AMUSIA M. YA., MSEZANE A. Z. AND POPOV K. G., *Phys. Rep.*, **492** (2010) 31.
- [16] SHAGINYAN V. R., MSEZANE A. Z. AND POPOV K. G., *Phys. Rev. B*, **84** (2011) 060401(R).
- [17] YAN S., HUSE D. A. and WHITE S. R., *Science*, **332** (2011) 1173.
- [18] SHAGINYAN V. R., MSEZANE A. Z., POPOV K. G. and STEPANOVICH V. A., *Phys. Rev. Lett.*, **100** (2008) 096406.
- [19] V. LÖHNEISEN H., ROSCH A., VOJTA M. and WÖLFLE P., *Rev. Mod. Phys.*, **79** (2007) 1015.
- [20] JOMPOL Y. *et al.*, *Science*, **325** (2009) 597.
- [21] GEGENWART P. *et al.*, *New J. Phys.*, **8** (2006) 171.
- [22] LANDAU L. D., *Sov. Phys. JETP*, **3** (1956) 920.
- [23] CLARK J. W., KHODEL V. A. and ZVEREV M. V., *Phys. Rev. B*, **71** (2005) 012401.
- [24] KHODEL V. A., CLARK J. W. and ZVEREV M. V., *Phys. Rev. B*, **78** (2008) 075120.
- [25] SHAGINYAN V. R., POPOV K. G., STEPANOVICH V. A., FOMICHEV V. I. and KIRICHENKO E. V., *Europhys. Lett.*, **93** (2011) 17008.
- [26] IMAI T., NYTKO E. A., BARTLETT B. M., SHORES M. P. and NOCERA D. G., *Phys. Rev. Lett.*, **100** (2008) 077203.
- [27] CARRETTA P., PASERO R., GIOVANNINI M. and BAINES C., *Phys. Rev. B*, **79** (2009) 020401(R).
- [28] KHODEL V. A. AND SCHUCK P., *Z. Phys. B*, **104** (1997) 505.